ADVANCED MATERIALS

www.advmat.de

Interface Engineering for Garnet-Based Solid-State Lithium-Metal Batteries: Materials, Structures, and Characterization

*Jiaqi Dai, Chunpeng Yang, Chengwei Wang, Glenn Pastel, and Liangbing Hu**

Lithium-metal batteries are considered one of the most promising energy-storage systems owing to their high energy density, but their practical applications have long been hindered by significant safety concerns and poor cycle stability. Solid-state electrolytes (SSEs) are expected to improve not only the safety but also the energy density of Li-metal batteries. The key challenge for solid-state Li-metal batteries lies in the low ionic conductivity of the SSEs and moreover the interface contact between the electrode and SSE. To achieve feasible solid-state Li-metal batteries, it is imperative that the ionic conductivity is improved, especially at the electrode–SSE interface. Herein, recent advances in interface engineering for solid-state Li-metal batteries are reported, mainly focusing on garnet-type SSEs. Various materials to modify the cathode–garnet and Li–garnet interfaces by intermediate layers, alloys, and polymer electrolytes are analyzed. Structural innovations for SSEs including composite electrolytes and multilayer SSE frameworks are reviewed, along with advanced characterization approaches to probe the interfaces, which will provide further insights for garnet-based solid-state batteries. Future challenges and the great promise of garnet-based Li-metal batteries are discussed to close.

1. Introduction

Lithium-metal batteries, such as lithium–sulfur batteries and lithium–air batteries, have attracted tremendous interest owing to their extremely high energy density. Deemed the "Holy Grail" of Li-ion batteries, metallic Li anodes provide the lowest electrochemical potential (−3.04 V against the standard hydrogen electrode) and highest specific capacity (3860 mAh g^{-1}). Its application, however, is greatly hindered by its huge volume change during cycling and dendrite growth caused by uneven Li plating. Especially in conventional batteries with organic liquid electrolytes, Li dendrites can grow and propagate to gradually penetrate the separator, resulting in severe short-circuit-induced safety issues. Therefore, conventional liquid electrolytes have quickly become inadequate for the application of Li-metal anodes due to these safety concerns. Their electrochemical and thermal stability, flammability, and mechanical strength do not meet the needs of today's consumers.

Replacing liquid electrolytes with solid-state electrolytes (SSEs) can not only address the aforementioned safety concerns but also enable the practical application of Li-metal anodes and high voltage cathodes to achieve higher energy and power densities. Since the discovery of the Ag_2S and PbF_2 in the early 19th century, research on SSEs has focused on searching for fast ion conductors with outstanding ionic conductivity, electrochemical stability, and mechanical strength. Today, numerous inorganic Li-ion conductive materials have been reported,[1] including but not limited to garnets,[2–6] perovskites,[7–9] sulfides,[10,11] and hydrides.[12–14] Among the various Li-ion conductors, garnet-type $Li_7La_3Zr_2O_{12}$ (LLZO) exhibits high Li-ion conductivity, outstanding electrochemical stability with a wide operating voltage window, relatively good chemical stability, and robust mechanical strength.[15,16] Thus, intensive studies have been devoted to solid-state Li batteries with garnet-type SSEs (**Figure 1**).

In addition to the persistent exploration of super-ionic conductors,[18] the research focus of SSEs has expanded to encompass the fundamental ion-transport mechanisms at interfaces that enable successful integration of SSEs in full cells. In particular, the high interfacial impedance and low interface stability of solid-state batteries has long thwarted the performance of SSEs. Due to insufficient solid–solid contacts between inorganic SSEs and solid electrodes, the interfacial impedance in solid-state Li batteries can be two to three orders of magnitude greater than Li-ion batteries with organic electrolytes. This value can also increase dramatically over long-term cycling and greatly hamper battery cycle life. Thus, the SSE–electrode interface problem has become the grand challenge in solid-state Li-metal batteries. Herein, we will focus on reviewing the recent advances in negating interfacial impedance in solid-state Li-metal batteries at both the interfaces between the electrolyte and electrodes and the interfaces within the electrolyte, from the perspective of materials development and structure design. Advanced characterization techniques for understanding solid interfacial reactions are also highlighted, which will facilitate future development of solid-state batteries.

Dr. J. Dai, Dr. C. Yang, Dr. C. Wang, G. Pastel, Prof. L. Hu
Department of Materials Science and Engineering
University of Maryland
College Park, MD 20742, USA
E-mail: binghu@umd.edu
Dr. J. Dai, Dr. C. Yang, Dr. C. Wang, G. Pastel, Prof. L. Hu
Maryland Energy Innovation Institute
University of Maryland
College Park, MD 20742, USA

The ORCID identification number(s) for the author(s) of this article can be found under https://doi.org/10.1002/adma.201802068.

DOI: 10.1002/adma.201802068

2. Materials Selection for Electrolyte–Electrode Interfaces

2.1. Anode (Li-Metal)–Electrolyte Interface

One of the main advantages of an SSE, especially a garnet-based SSE, is the safe implementation of Li-metal anodes. However, the poor contact between the Li-metal foil and garnet SSE results in large interfacial resistance, even when applying pressure at the softening temperature.[19,20]

The successful demonstration of a solid-state Li battery using garnet electrolytes, reported by van den Broek et al., pointed out that the contact at the anode–electrolyte interface is crucial to ion transport.[21] By intimately embedding nanograined anode materials into the porous electrolyte interlayer, this work greatly expanded the effective contact area, resulting in a significant reduction in interfacial resistance. The interface-engineered garnet cells developed in this work provide guidelines for improving solid-state batteries through interface engineering. To achieve sufficient contact, it is vital for lithium to fully wet the surface of garnet. However, experiments have shown that molten Li has poor wettability against garnet SSE. The wetting behavior is fundamentally determined by the surface energy mismatch associated with the respective SSE and metallic Li anode. Therefore, wetting can be improved through two routes. The first route is to modify the SSE surfaces to minimize the difference in surface energy. The second route, however, is to tune the surface energy of the metallic Li anode to match that of the garnet surface.

Following the first route, in which the SSE surfaces are modified, several studies have addressed the Li wetting issue through surface modification. The first successful demonstration introduced an ultrathin Al_2O_3 coating on SSEs through atomic-layer deposition (ALD). Han et al. reported that a 5 nm coating of Al_2O_3 led to a great improvement in the wetting of Li metal to the SSE and a dramatic decrease in in the interfacial resistance.[22] The drop in interfacial resistance results from the elimination of voids at the interface between the garnet and the Li metal (**Figure 2**a). The ultrathin Al_2O_3 layer improves the wettability of the molten Li metal by tuning the surface energy of garnet to match that of molten Li (Figure 2b). The effect of ALD on the garnet/Li interface was evaluated quantitatively by electrochemical impedance spectroscopy (EIS). The calculated total area specific resistance (ASR) was 176 Ω cm^2 for the ALD-treated sample, which is significantly lower than that of the sample without ALD treatment (3528 Ω cm^2) (Figure 2c). The ALD treatment reduced the interfacial ASR from 1710 Ω cm^2 to 34 Ω cm^2. It was postulated that Al_2O_3 is lithiated by contact with molten Li metal, thereby forming an ionically conductive layer that can not only effectively transport ions between the garnet and Li metal, but also mitigates impurities and defects such as Li_2CO_3 patches and surface cracks at the interface. The reliability of the ALD-Al_2O_3 method was examined by direct current (D.C.) Li plating and stripping. Figure 2d,e compare the D.C. cycling performance of Li/bare-garnet/Li and Li/ALD-treated-garnet/Li symmetric cells. The ALD-Al_2O_3 sample demonstrates stable cycling performance, which addresses the main challenge of interfacial impedance and interface stability with the anode.

Jiaqi Dai received his B.S. degree from Harbin Institute of Technology, China, in 2013 and his Ph.D. degree in materials science and engineering from the University of Maryland, College Park, in 2018. He is currently a postdoctoral researcher in the group of Prof. Liangbing Hu in the Maryland Energy Innovation Institute. His research mainly focuses on solid-state energy-storage devices, nanomaterials and nanostructures, and scientific visualizations.

Chunpeng Yang received his B.S. degree from the University of Science and Technology of China in 2011 and his Ph.D. degree from the University of Chinese Academy of Sciences in 2016. He is currently a postdoctoral researcher in the group of Prof. Liangbing Hu at the University of Maryland, College Park. His research focuses on materials for advanced energy-storage systems, such as lithium-metal batteries and solid-state batteries.

Liangbing Hu received his B.S. degree in applied physics from the University of Science and Technology of China (USTC) in 2002. He did his Ph.D. with Prof. George Gruner at UCLA, focusing on carbon-nanotube-based nanoelectronics. In 2006, he joined Unidym Inc as a cofounding scientist and worked on printed carbon-nanotube transparent electrodes and device integration. He did his postdoc with Prof. Yi Cui at Stanford University from 2009–2011. Currently, he is an associate professor at the University of Maryland, College Park. His research interests include nanomaterials and nanostructures, flexible and printed electronics, energy storage and conversion, and roll-to-roll nanomanufacturing.

In addition to Al_2O_3, ZnO has also been reported to improve the wettability and reduce the Li–garnet interfacial resistance. Compared to Al_2O_3, ZnO has a higher chemical reactivity to the molten Li, which provides an additional driving force to coat the surface of the garnet SSE. Wang et al. demonstrated much improved Li wetting behavior on garnet with a thin layer of

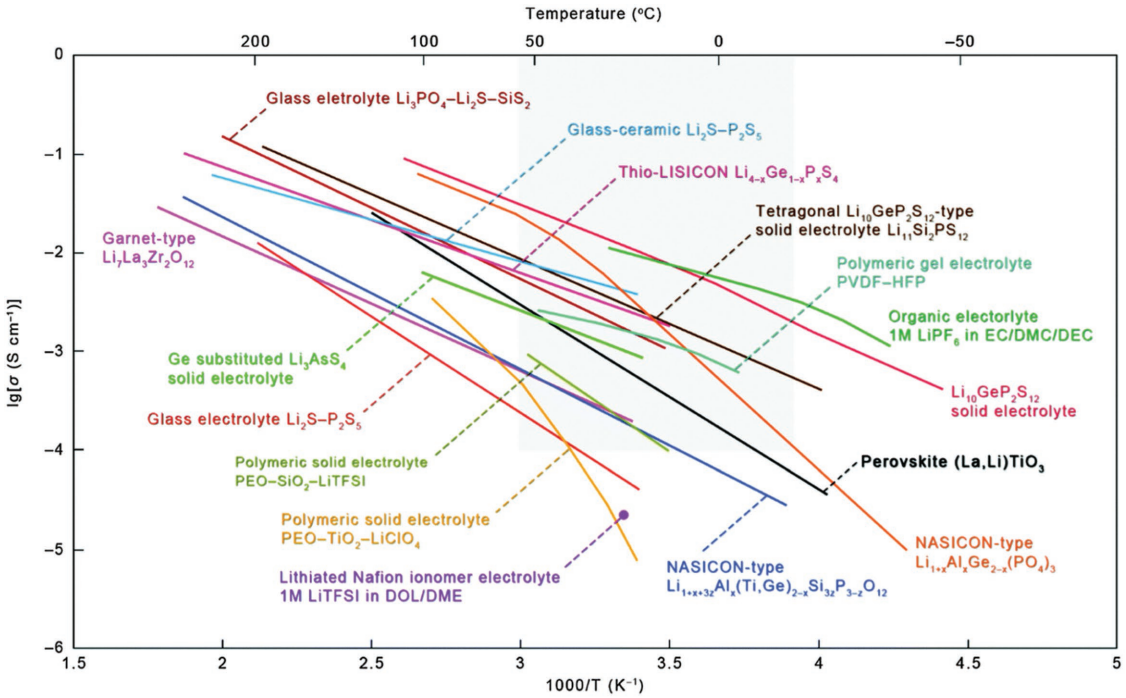

Figure 1. The relationship between the ionic conductivity and temperature of different types of electrolytes. Reproduced with permission.[17] Copyright 2015, the Royal Society of Chemistry.

ZnO coated by ALD (Figure 2f).[23] In this work, the conformal ZnO coating enabled molten Li to wet the garnet surface and flow into a highly tortuous 3D porous garnet SSE structure (Figure 2h–j). The flow of molten lithium into the complex 3D anode frameworks (lithium hosts), as driven by wetting on ZnO and other materials, opens many opportunities for controlling lithium deposition and suppressing dendrite formation.[24,25]

Even though ALD is very effective at improving Li wettability of garnet SSE, it still remains an expensive process. The high environmental requirement (vacuum, clean surface) and long processing time result in a high manufacturing cost for garnet solid-state batteries, which makes ALD a less favorable technique for large-scale production. In addition, the synthesis, transport, and storage of the highly reactive and often air-sensitive precursors further increases the manufacturing costs associated with ALD. In addition, garnet surface modifications using ALD are also limited by the available precursors. Therefore, to address the wetting issue of garnet SSE through surface coating, more cost-effective deposition methods (e.g., chemical vapor deposition (CVD)[26,27]) and coating materials need to be explored.

In contrast to the first route, the second route modifies the metallic Li anode directly. This route is free of the abovementioned technical limitations, which offers more opportunities to incorporate various processing techniques and a wider selection of additive materials. Following the second route, several alloying methods have been reported to address the wetting issue between molten metals and ceramic substrates. Wang et al. reported a Li–Sn alloy that can greatly improve the wettability of molten lithium on a garnet SSE.[28] An alloy with 30–50 wt% of Sn sufficiently wets the surface of the alumina (or garnet) substrate in a short time (less than 10 s, **Figure 3**a,b) with an almost negligible contact angle. The SEM images in Figure 3c,d reveal the Li–Sn fully wetting the substrate surface, including dents and cracks. The significantly improved contact resulted in an interfacial resistance as low as ≈7 Ω cm^2.[28] Similarly, Li–Al and Li–Ge alloys also exhibit excellent wetting properties on garnet surfaces.[29–31] The outstanding wetting performance of Li alloys enables the direct coating of molten lithium onto garnet SSE, which greatly reduces manufacturing cost and processing time. Therefore, the alloying method shows great potential for the fabrication of large-scale solid-state battery systems.

Given the clear advantages of the alloying method, it is also essential to point out that many electrochemical and interfacial properties related to lithium alloys in solid-state batteries remain unclear. Compared with ceramic/metal-alloy composites, whose wetting-property–composition relationship has been well studied both experimentally and computationally,[32–34] current garnet/Li-alloy interface studies lack rigorous theoretical insights. For example, the surface properties of Li–Al and Li–Zn alloys have been thoroughly studied theoretically,[35] but the relationship between the chemical and electrochemical stability of garnet against various alloy compositions is yet to be explored. Therefore, theoretical studies on the garnet/lithium-alloy interfaces, including calculation of phase diagrams and computational simulations, are critical to the development of a comprehensive alloying method for garnet SSEs in the future.

2.2. The Cathode–Electrolyte Interface

To construct solid-state batteries, it is also vital to improve the cathode–electrolyte interface, including electron transference across the cathode and ion conductivity across the solid–solid

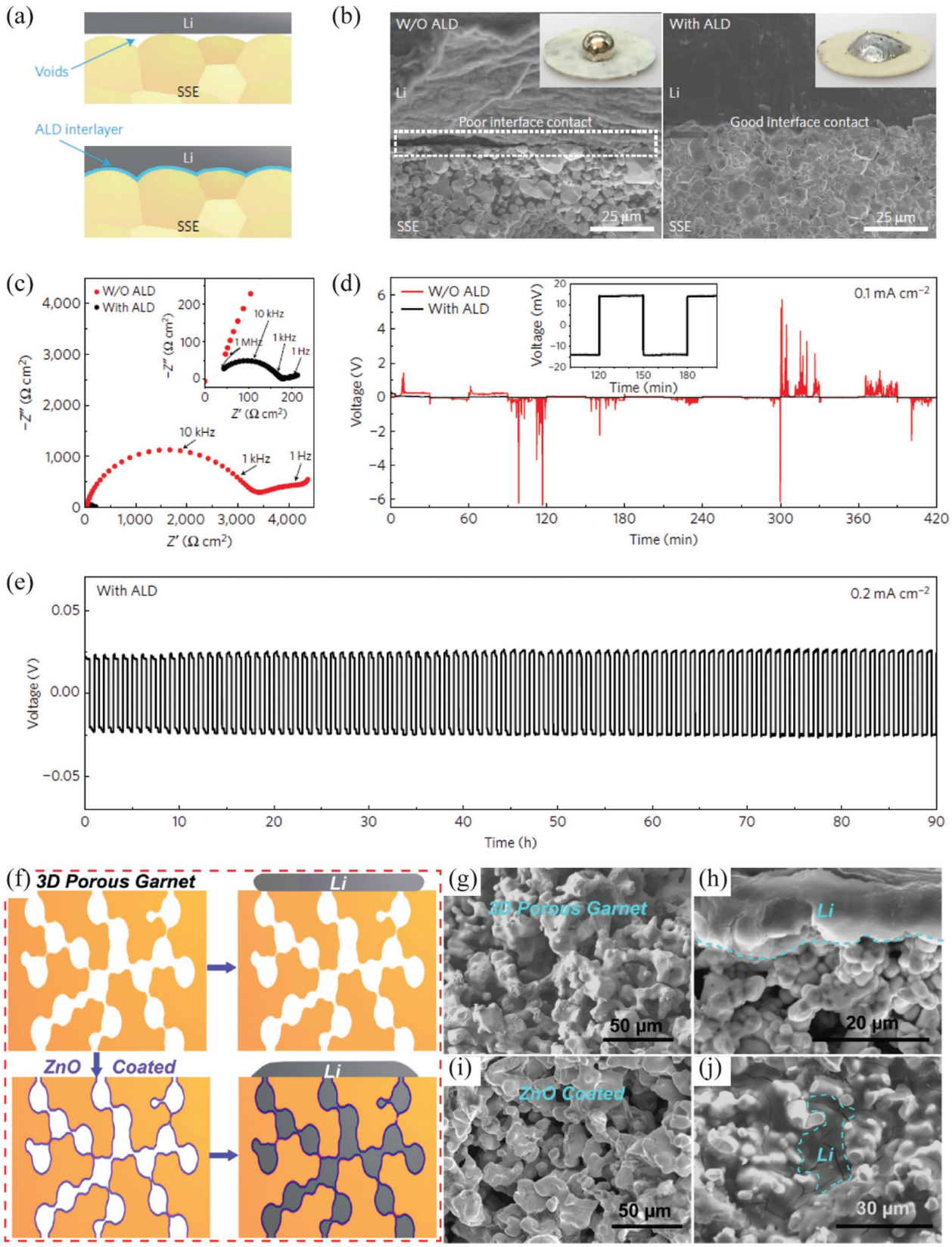

Figure 2. Improved lithium wetting through surface modifications. a) Schematic comparing the wetting behavior of molten lithium on bare and ALD-treated garnet surface. b) SEM and optical microscopy images (insets) of the garnet solid-state electrolyte/Li–metal interface showing the uniform

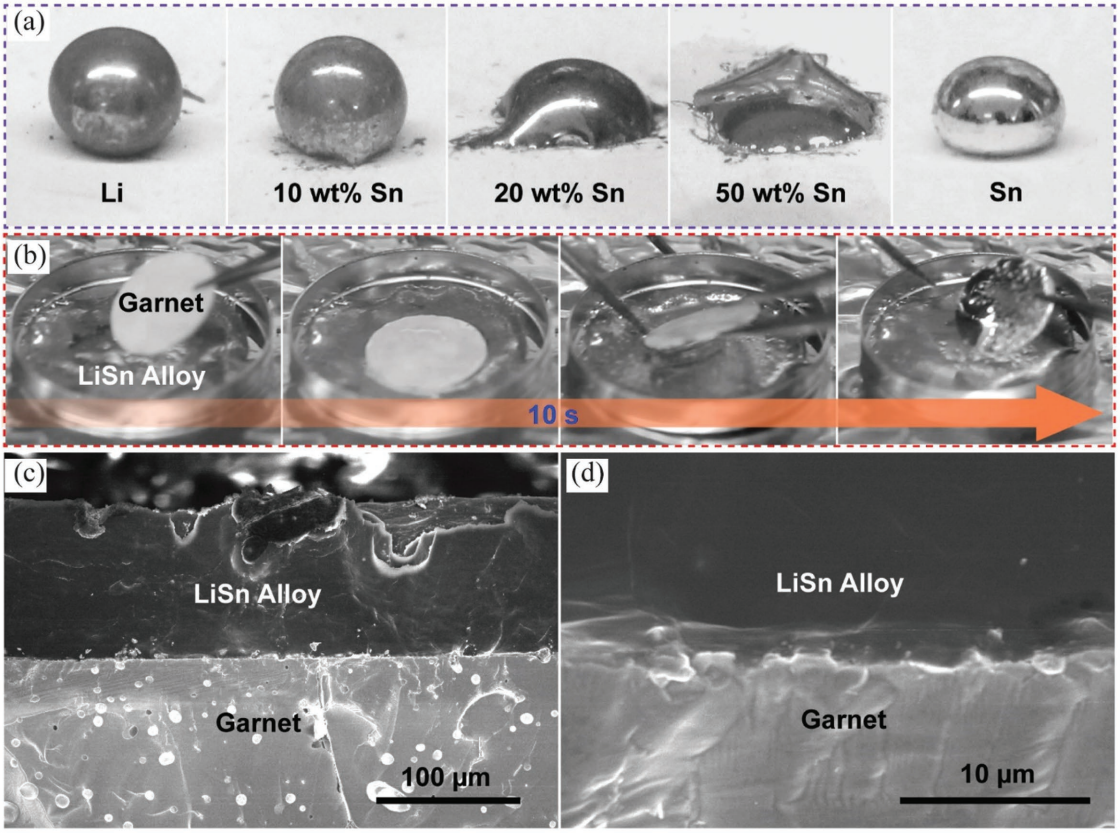

Figure 3. Improving lithium wetting on garnet with a Li–Sn alloy. a) Wettability on an alumina substrate of molten Li–Sn alloys of various Sn contents. b) Images demonstrating the short timescale for wetting the Li–Sn alloy on a bare garnet surface. c,d) Cross-sectional SEM images of the garnet pellet coated with the Li–Sn alloy at low and high magnification, which indicate a conformal interface between the alloy and garnet SSE. Reproduced with permission.[28] Copyright 2017, Wiley-VCH.

interface. The solid–solid cathode–SSE interface, which is inherently highly resistive, significantly hampers electron and ion transport during the respective electrochemical reaction(s). A straightforward but compromising approach to reduce the solid–solid interfacial resistance employs a solid polymer electrolyte as an interlayer to cushion the poor contact between the rigid cathode and ceramic electrolyte.

Goodenough and co-workers pioneered the polymer/ceramic/polymer sandwich electrolyte for solid-state Li batteries.[36] They used cross-linked poly(ethylene glycol) methyl ether acrylate as a polymer Li-ion conductor to sandwich a ceramic membrane of Na super ionic conductor (NASICON) type SSE (**Figure 4**a). On the Li-anode side, the polymer electrolyte reduces the Li-ion transfer resistance and distributes the Li-ion flux more uniformly. On the cathode side, the cross-linked polymer electrolyte serves as binder and an ion conductor for the $LiFePO_4$ cathode. As shown in Figure 4b, the resultant solid-state Li/$LiFePO_4$ cell with the sandwich electrolyte shows a flat charge/discharge plateau and high Coulombic efficiency, which attests to the merit of a polymer/ceramic hybrid electrolyte for solid-state batteries. This method was also extended to garnet-type SSE, with a cross-linked PEO polymer electrolyte as a buffer layer for the Li anode and $LiFePO_4$ cathode.

While the polymer–ceramic electrolyte integrates the advantages of solid polymer electrolytes and ceramic electrolytes, its thickness has to be reduced for lower electrolyte impedance. The polymer layers are not rigid enough to suppress Li dendrites. In contrast to the symmetric sandwich structure, Guo and co-workers designed a polymer–ceramic asymmetric solid electrolyte, which was composed of a rigid ceramic layer facing the Li-metal anode and a soft polymer layer to improve the cathode–SSE contact.[37] As shown in Figure 4c, the dense and thin garnet ($Li_7La_3Zr_2O_{12}$) layer can block Li penetration while the soft layer of poly(ethylene glycol) methyl ether

bonding of lithium and garnet with the ALD-Al_2O_3 coating. c) EIS profile comparison of the symmetric Li nonblocking garnet cells. The inset shows a zoomed-in view of the high-frequency region. d) D.C. cycling comparison for symmetric Li nonblocking cells with bare garnet and surface-treated garnet as electrolytes. e) Galvanostatic cycling of a symmetric cell with metallic lithium electrodes and surface-treated garnet electrolyte. a–e) Reproduced with permission.[22] Copyright 2016, Springer Nature. f) Schematic showing lithium infiltration into porous garnet with or without surface modification. Cross-sectional SEM image of the g) preinfiltration and h) postinfiltration pristine porous garnet with a porosity of 60–70%. i,j) Cross-sectional SEM image of i) preinfiltration and j) postinfiltration surface-treated porous garnet with improved wetting due to the ZnO coating. f–j) Reproduced with permission.[23] Copyright 2017, American Chemical Society.

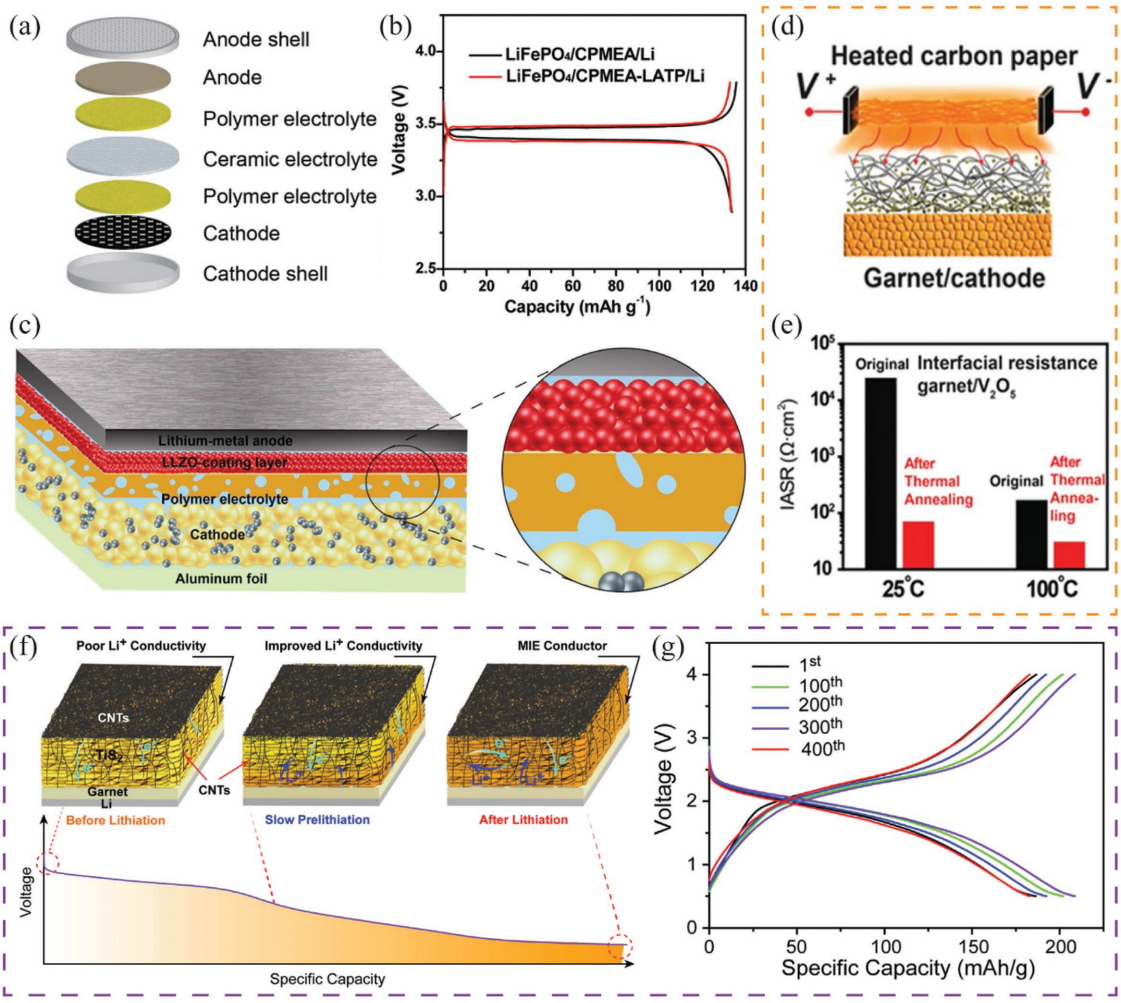

Figure 4. Strategies to improve the cathode–electrolyte interface. a) Schematic illustration of the solid-state cell composition with the polymer/ceramic/polymer sandwich electrolyte. b) Charge/discharge voltage profiles of Li/$LiFePO_4$ cells at 0.2C using the cross-linked poly(ethylene glycol) methyl ether acrylate (CPMEA) polymer electrolyte with or without LATP ceramic electrolyte. a,b) Reproduced with permission.[36] Copyright 2018, American Chemical Society. c) Schematic of the asymmetric solid Li-metal battery design with a rigid ceramic layer modified with an ultrathin polymer by the Li-metal anode and a soft polymer layer contacting the cathode. c) Reproduced with permission.[37] Copyright 2018, American Chemical Society. d) Schematic of the method to improve the solid-electrolyte–cathode interface by rapid thermal annealing. e) Comparison of the charge-transfer impedance at the garnet–cathode interface at 25 and 100 °C before and after the thermal annealing. d,e) Reproduced with permission.[42] Copyright 2017, American Chemical Society. f) Schematic of the Li–garnet–TiS_2 solid-state battery and the prelithiation process. g) Voltage profiles of the solid-state battery using a prelithiated TiS_2 cathode cycled under 300 mA g^{-1} (until the 100th cycle), 500 mA g^{-1} (until the 300th cycle), and 1000 mA g^{-1} (until the 400th cycle) at 150 °C. f,g) Reproduced with permission.[43] Copyright 2018, Elsevier Ltd.

acrylate ameliorates the cathode–SSE interface connection and facilitates Li-ion transport. The asymmetric electrolyte is thin, with a 5.7 µm garnet layer and 5.4 µm polymer layer, resulting in a low-interfacial-area specific resistance. Similar polymer-enhanced cathode–SSE interfaces have been widely reported.[38,39] Even though polymer interlayers can cushion the rigid interface and constrain liquid electrolyte, they lower the energy density due to the additional weight of inactive materials. In addition, polymer–ceramic or liquid–ceramic hybrid electrolytes also undermine the nonflammability and thermal stability of inorganic SSEs. These disadvantages lead to the need of liquid-free techniques for interface modifications.

Li_3BO_3 has been reported as a solid electrolyte to improve the interface between garnet and the cathode, particularly $LiCoO_2$, for rechargeable solid-state Li-ion batteries.[40,41] Li_3BO_3 is a lithium-ion conductor and is chemically stable with the $LiCoO_2$ cathode material and garnet SSE. By sintering Li_3BO_3 into the cathode layer, sufficient interface contact with physical bonding and chemical interaction can be achieved between the cathode material and the garnet SSE. The resultant battery exhibited good electrochemical performance and a lower interfacial resistance comparable with that of lithium-ion batteries with liquid organic electrolytes.

Recently, our group developed a rapid thermal annealing method to fabricate all-solid-state batteries with low interface resistance and high-temperature performance.[42] The cathode material V_2O_5 was rapidly heated and coated on the garnet electrolyte with good interfacial wetting (Figure 4d). The V_2O_5

melts at 690 °C and is stable during the thermal annealing. Thus, it can be melted and re-solidifies on the garnet interface after the thermal annealing to improve the contact with the garnet SSE. The garnet–V_2O_5 shows significantly reduced interfacial resistance after thermal stabilization and the crystalline structure and chemical state of the V_2O_5 remain unchanged (Figure 4e). The all-solid-state full cell exhibits stable cycling performance at 100 °C and the garnet–V_2O_5 is nonflammable, thereby demonstrating the superb safety of the respective solid-state batteries.

Instead of direct modifying the interfaces, the use of mixed ionic–electronic (MIE) conductor targets at the cathode material provides an alternative route to improve the cathode–SSE interface. Wang et al. reported that the use of an MIE conductor, TiS_2, as cathode reduced the cathode–SSE interfacial resistance by more than 20 times.[43] The two-dimensional (2D) layered TiS_2 shows a sufficient MIE conductivity after a simple slow prelithiation process (Figure 4f), which can greatly promote the electrochemical reactions at the cathode. A full cell using the MIE conductor cathode showed stable cycling performance at high current density with a high capacity of ≈200 mAh g^{-1} at 150 °C (Figure 4g). This unique strategy of using a 2D MIE conductor to address the interface challenges can not only be generalized to many other cathode chemistries, but also provides a novel perspective on cathode–SSE interface enhancement through modifications targeting the cathode material itself.

With growing understanding of the ion-transport mechanism at the cathode–SSE interfaces, more and more interfacial modification techniques are being developed to address the critical challenges of transferring ions into the solid-state cathode. For example, further development of solid-state cathode materials by in situ synthesis and co-sintering on garnet SSE is appealing to form a more continuous solid-state conductive framework with the cathode. As nanostructures can significantly reduce the solid-state ion-transfer path, innovative designs of nanostructured cathode–SSE architectures can be an effective approach for solid-state batteries.

3. Structural Design for Interfaces within Electrolytes

Aside from the above dense and planar garnet electrolyte architectures, construction of complex 3D garnet frameworks has garnered great interest. For instance, garnet frameworks can be filled with a polymer electrolyte to form composite electrolytes with better integrity and overall performance than their laminated counterparts. For these composite electrolytes, the interface between the component phases is a determining factor for the overall ionic conductivity and electrochemical stability. Therefore, current research focuses on identifying the role of interfaces in ion transport, investigating interface stability via computational simulations, and manipulating interfaces through structural designs to achieve the optimal conductivity

To build garnet composite electrolytes, garnet can be dispersed as a filler in the form of connected particles, interconnected nanofibers, or preferably, aligned nanofibers in the polymer electrolyte (**Figure 5**a–c). In keeping with the percolation effect, to obtain high ionic conductivity, garnet nanoparticles in a polymer matrix should be small with high specific surface area. A composite electrolyte with garnet nanoparticles of ≈40 nm diameter (Figure 5d) exhibited a conductivity of 2.1×10^{-4} S cm^{-1} at 30 °C, almost two orders of magnitude greater than that with 10 μm garnet particles (Figure 5e).[44] The enhanced ionic conductivity of the composite electrolyte with nanoscale garnet particles is attributed to the increase in coherent conductivity paths along the interfaces between the PEO and garnet grains. In addition to the particle size, the weight ratio of garnet in the composite electrolyte plays an important role in the properties and performance of the composite electrolyte. An electrolyte consisting of more polymer than ceramic, or "polymer-in-ceramic" electrolyte has better flexibility, while ratios with more ceramic, or "ceramic-in-polymer" electrolytes show higher mechanical strength and safety.[45]

Compared to particle fillers, garnet–nanofiber frameworks can provide longer ion-transfer channels with fewer grain interfaces. Fu et al. reported a flexible garnet–polymer composite electrolyte membrane based on garnet nanofibers.[46] The garnet nanofibers (Figure 5f) were fabricated using electrospun polymer fibers as a template. The resultant composite electrolyte was obtained by directly soaking the garnet-nanofiber framework in a polymer electrolyte solution. The composite electrolyte, consisting of a garnet-nanofiber network, exhibited not only a high ionic conductivity of 2.5×10^{-4} S cm^{-1} at room temperature (Figure 5g) but also good thermal stability, low flammability, and chemical stability against Li, air, and moisture.

Inspired by the PEO–garnet-nanofiber composite electrolyte,[46] many polymer–ceramic electrolytes have been reported using different 3D ceramic SSEs, such as bacteria-cellulose-templated garnet nanofibers.[47,48] For polymer electrolyte with nonconductive fillers, the enhanced conductivity is mainly attributed to the reduced crystallinity of the polymer electrolyte. With garnet as the filler, however, the Li-ion conductive network provides additional ion pathways. Solid-state Li NMR proves that Li ions are transported through the garnet ceramic phase instead of the PEO–garnet interface or the PEO electrolyte.[49] Therefore, aligned ceramic SSE nanowires that are normal to the electrode are expected to enhance the ionic conductivity of the polymer–ceramic composite electrolyte beyond that of a random nanofiber network. This speculation has been demonstrated by Cui and co-workers.[50] Aligned ceramic SSE nanowires ($Li_{0.33}La_{0.557}TiO_3$) were fabricated on Pt electrodes by electrospinning (Figure 5h) and formed a composite electrolyte with a PAN-based electrolyte. The conductivity of the composite electrolyte with aligned ceramic SSE nanowires at different orientations (e.g., 0° indicates nanowires along the normal direction of the Pt electrodes) is summarized in Figure 5i in comparison with random garnet nanowires and other electrolytes. The electrolyte with aligned garnet nanowires (normal to the electrode, along the ion-transport direction) exhibits the highest ionic conductivity, 6.05×10^{-5} S cm^{-1} at 30 °C, one order of magnitude higher than that of random garnet nanowires. These results strongly suggest that the fast ion-conducting pathways, without crossing junctions on the surfaces of the aligned nanowires, can contribute significantly to the overall conductivity. Similar conclusions have been found

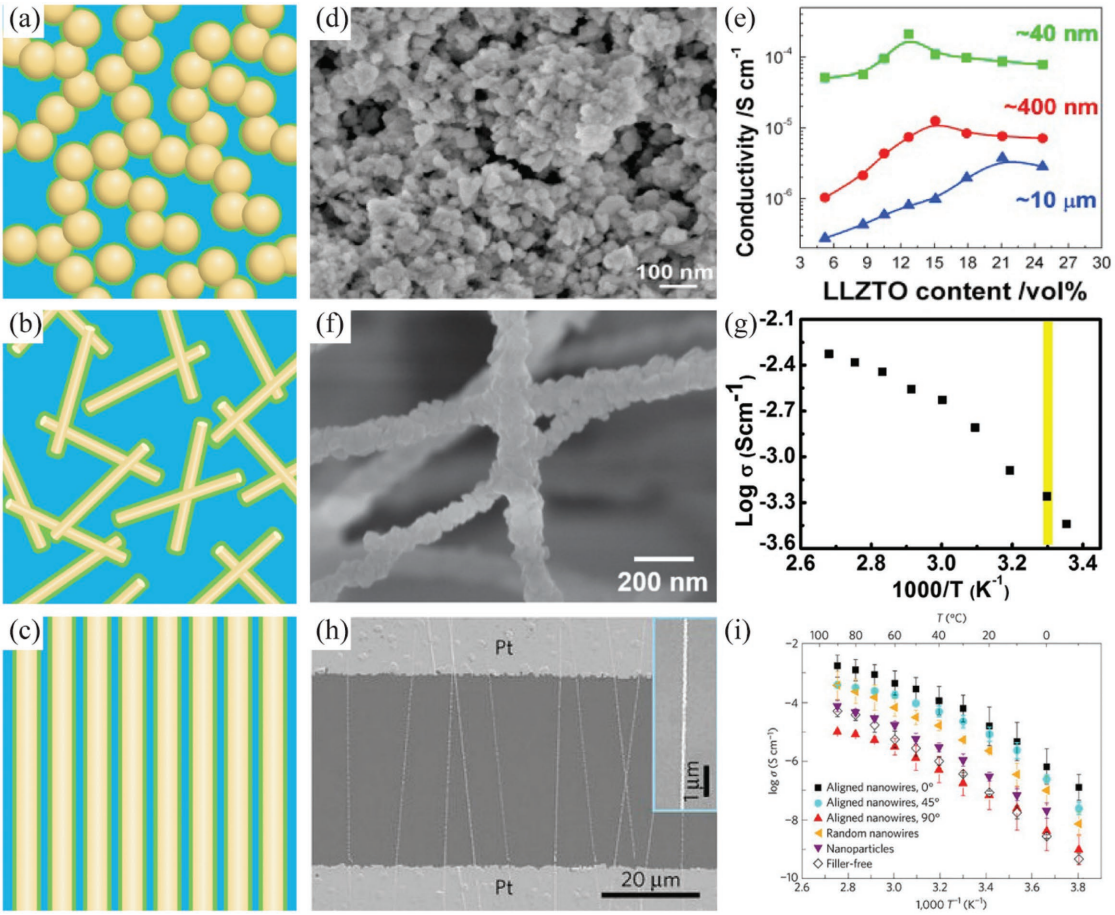

Figure 5. Constructing polymer–ceramic composite solid electrolytes. a–c) Schematics of the structure of and ion transfer through polymer–ceramic composite electrolytes with: a) dispersed ceramic SSE nanoparticles, b) random ceramic SSE nanofibers, and c) aligned ceramic SSE nanofibers. d) SEM of garnet nanoparticles with an average size of 40 nm. e) Ionic conductivity of the PEO–garnet composite electrolyte with various garnet particle sizes. d,e) Reproduced with permission.[44] Copyright 2016, Elsevier. f) SEM image of the garnet nanofibers derived from electrospun polymer nanofiber template. g) Temperature dependence of the ionic conductivity of the PEO–garnet nanofiber composite (from 20 to 90 °C). f,g) Reproduced with permission.[46] Copyright 2017, National Academy of Sciences. h) SEM image of the aligned SSE nanowires on a quartz substrate with Pt electrodes at a nanowire orientation of 0°. i) Temperature dependence of the ionic conductivity in the composite electrolytes with aligned ceramic nanowires (at different orientations), random ceramic nanowires, ceramic nanoparticles, and free from fillers. h,i) Reproduced with permission.[50] Copyright 2017, Nature Publishing Group.

in a composite electrolyte with vertically aligned ceramic electrolyte ($Li_{1+x}Al_xTi_{2-x}(PO_4)_3$), which was fabricated using an ice template.[51] Although the aligned SSEs were not garnet electrolyte, the results clearly show that integrating vertically aligned ceramic SSE nanowires with a polymer electrolyte favors ion conductivity and combines the merits of ceramic and polymer electrolytes. Though the composite electrolytes reported by Cui and co-workers were small-scale for material characterization, the enhancement demonstrated by manipulating nanowire orientations is likely to inspire future development of composite electrolytes using aligned-single-nanowire arrays. In addition, the aligned nanowires eliminate potential interference from the electrolyte structures, which will provide a great tool for future interface studies. Given that the ion-transport behavior in composite electrolytes remains controversial, opportunities await in both experimental and theoretical studies to not only clarify the role of interfaces in conductivity enhancement, but also to predict, design, and select materials for the optimum interfaces.

Instead of filling 3D garnet frameworks with polymer electrolyte, the frameworks can be directly applied as an ionically conductive host for Li-metal anode or cathode materials. Compared with the above planar SSEs, porous garnet frameworks can provide sufficient interfacial contact and volume to host electroactive material. Recently, porous garnet frameworks have been reported as a host for solid-state Li batteries.[52,53] The SEM image in **Figure 6**a displays the structure of the solid-state garnet framework, in which the porous garnet is sintered with a dense layer and forms a porous–dense bilayer structure.[52] The dense layer is thin but critical to separate the cathode and anode. The sintered solid host also minimizes the ionic resistance at the dense–porous interface. In this design, the porous layer can be thick to host active material with high mass loading. As shown in Figure 6b, with the porous–dense bilayer framework, Li adheres to the dense layer via the aforementioned surface-treatment method (adding a polymer-electrolyte layer), and CNTs and sulfur are infiltrated into the porous garnet

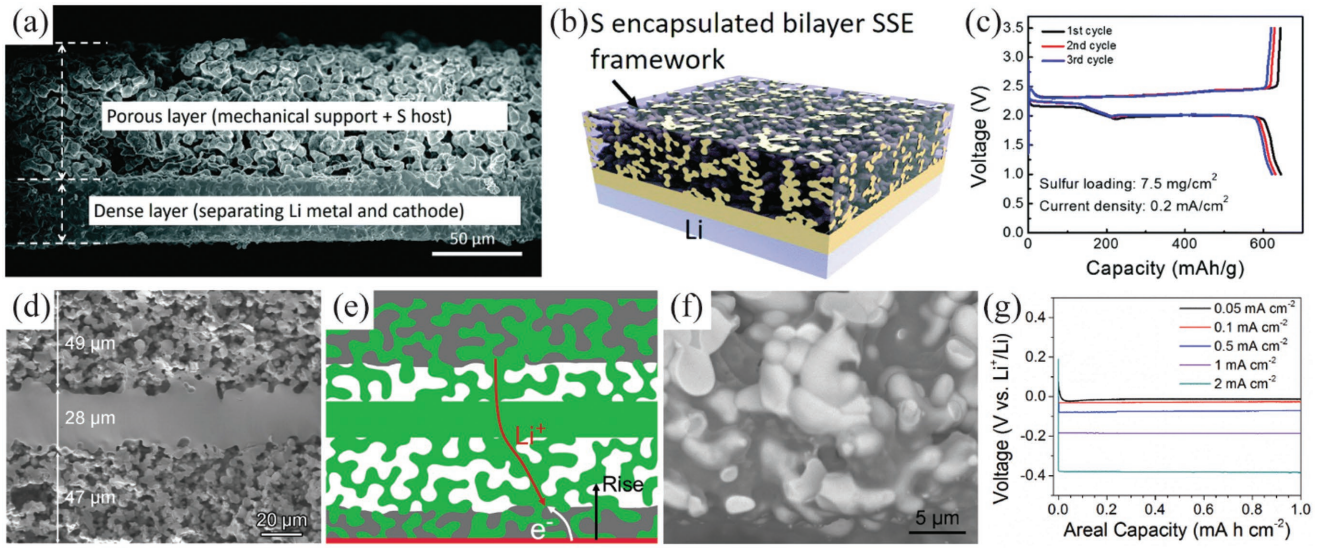

Figure 6. 3D garnet framework for solid Li-metal batteries. a) Cross section of the porous–dense bilayer garnet framework. b) Schematic of the Li–S battery with S encapsulated in the porous garnet framework and Li on the dense side of the garnet. c) Discharge/charge voltage profiles of the Li–S battery based on the bilayer garnet at 0.2 mA cm^{-2} with a high S mass loading. a–c) Reproduced with permission.[52] Copyright 2017, Royal Society of Chemistry. d) Cross section of the porous–dense–porous trilayer garnet framework. e) Schematic of the solid plating behavior of the Li-metal anode in the trilayer garnet framework with a bottom coated Cu layer. f) SEM image of Li deposited at the bottom of the trilayer garnet framework, where garnet is bright and Li is dark. g) Voltage profiles of 1 mA h cm^{-2} of Li plating within the trilayer garnet at various current densities. d–g) Reproduced with permission.[53] Copyright 2017, National Academy of Sciences.

layer. In the porous layer, the CNT conducts electrons and the 3D garnet conducts Li ions. The S distribution in the garnet framework can be clearly observed by SEM and elemental mapping. The S loading can be as high as 7.5 mg cm^{-2} while still delivering relatively high electrochemical activity, exhibiting a capacity of 645 mA h g^{-1} at 0.2 mA cm^{-2} (Figure 6c). The porous garnet framework introduces an effective strategy to address the electron/ion exchange interface in the solid-state cathode.

The porous–dense-bilayer garnet framework can be further developed for porous–dense–porous trilayer frameworks with the two porous layers hosting the cathode and Li anode, respectively. The plating/stripping behavior of the solid Li anode in the trilayer garnet framework has been recently reported.[53] The structure of the trilayer garnet framework is shown in the cross-sectional SEM image in Figure 6d, in which the dense layer has good integrity with the porous layers to reduce ion-migration impedance and block electron transfer. The solid ion-conductive framework is coated with a thin Cu layer for conducting electrons. Figure 6e schematically shows the Li-plating behavior in the trilayer garnet framework. Li is initially deposited on the bottom Cu layer and continuously rises during successive cycles of Li plating as confirmed by SEM of the Li-plated garnet framework (Figure 6f). The bottom-depositing behavior in the solid-state garnet host markedly precludes the formation of Li dendrites and eliminates Li penetration through the separator (dense layer). The 3D garnet host contributes additional ionically conductive surface area for the solid Li-metal anode and continuously hosts the anode during cycling. Thus, the Li anode in the trilayer garnet framework can be plated at relatively high current densities for 1 mA h cm^{-2} (Figure 6g), a capacity much greater than most previously reported all-solid-state Li anodes. Superb cycling performance has also been demonstrated by cycling at 0.5 mA cm^{-2} for 300 h. Using the porous ion-conductive framework to host the cathode and anode materials, the resultant solid-state Li batteries are largely exempt from volume-change effects and interface-contact issues during cell cycling, showing great promise for feasible solid-state Li batteries with high energy density.

4. Characterization Techniques

4.1. Electrochemical Impedance Spectroscopy

It is difficult to characterize elemental lithium by conventional techniques such as X-ray photoelectron spectroscopy and energy-dispersive X-ray spectroscopy. However, in Li-ion battery chemistries, Li is involved in the most critical processes that affect the battery performance; therefore, being able to "see" Li is key to optimizing battery chemistries and improving battery performance. In solid-state Li batteries, characterization can be more challenging. Therefore, SSEs are widely deemed "black boxes" for concealing the underling mechanisms and kinetics taking place. As a common electrochemical characterization technique, electrochemical impedance spectroscopy (EIS) is a useful tool to study interfacial processes and charge transfer through electrode materials. Even though the Li transport in solid-state batteries differs from liquid systems, EIS can still provide valuable information about the interfacial processes and Li^+ diffusion. Janek et al. systematically studied the interface between SSE and electrode materials at different states-of-charge (SOC) and states-of-discharge using EIS.[54] Two semicircles at low frequency and high frequency, corresponding to the anode/SSE and cathode/SSE interfaces, respectively, can

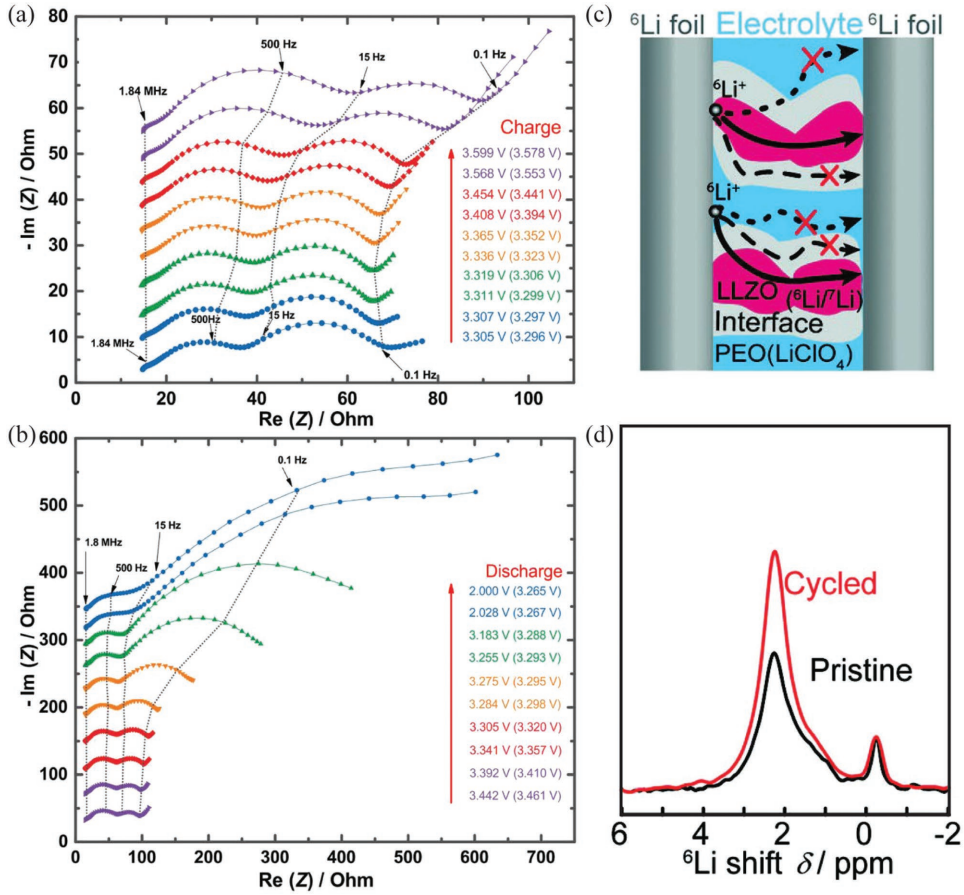

Figure 7. Characterization of solid-state batteries by EIS and NMR. a,b) Stacked Nyquist plots of an SSB with LNTO-coated $LiCoO_2$ as the active material during the charge (a) and discharge (b) process. Galvanostatic charge was carried out at 0.1C, and EIS was carried out after 1 h charge and 30 min rest. a,b) Reproduced with permission.[54] Copyright 2017, American Chemical Society. c) Illustration of the symmetric ^{6}Li-foil/composite electrolyte/^{6}Li-foil battery and possible Li^+-transport pathways within the composite electrolyte upon cycling the symmetric battery. d) Comparison of the ^{6}Li NMR spectra of the LLZO–PEO ($LiClO_4$) composite electrolytes before (pristine) and after cycling (cycled). c,d) Reproduced with permission.[56] Copyright 2016, Wiley-VCH.

be identified in all spectra acquired at different SOC (**Figure 7**a). The unchanged semicircles in the low-frequency range indicate a stable anode/SSE interface during the charging process. However, unlike the stable high-frequency semicircle corresponding to the SEI layer on $LiCoO_2$, and the decreasing mid-frequency semicircle indicating a semiconductor-to-metal phase transition in $LiCoO_2$ during delithiation,[55] the high-frequency semicircle related to the cathode/SSE interface in solid-state batteries slowly increases with increasing potential.[54] This abnormal cathode/SSE interface increase is attributed to the cracks in the amorphous coating due to the volume change of $LiCoO_2$. The cracks in the coating layer also result in an increased cell potential, which may initiate decomposition of the SSE, thereby further increasing the interfacial resistance. Another counterintuitive phenomenon pertains to the Warburg impedance, corresponding to the Li^+ diffusion in $LiCoO_2$ in the low-frequency region, which is larger at a high SOC and almost negligible at a low SOC. However, the chemical diffusion coefficient of Li^+ in LCO increases with SOC.[54]

During the discharge process, the cathode/SSE interfacial resistance remains almost constant, while the anode/SSE interfacial resistance increases. This indicates the resistance measured at the anode/SSE interface strongly depends on the amount of Li in the respective Li–In alloy (Figure 7b).[54] Therefore, in solid-state batteries, EIS still can qualitatively provide valuable information about the interfacial properties between the SSE and electrodes, as well as the Li^+-transport behavior between the electrode materials.

4.2. Nuclear Magnetic Resonance

To better understand the interfacial properties, quantitative characterization of the Li^+ transport in solid-state battery systems is exceedingly valuable. For this purpose, Hu et al. successfully implemented a high-resolution solid-state Li NMR study to investigate Li^+-transport behavior in cubic-phase LLZO-garnet–poly(ethylene oxide) (PEO) composite electrolytes.[56] With a unique isotope exchange strategy, the Li-ion-transport pathways within the composite electrolytes were successfully tracked and reported (Figure 7c). High-resolution NMR is sensitive enough to differentiate the

variation in the local structural environments of Li ions in the PEO phase, garnet phase, and garnet–PEO interface. By comparing the ^{6}Li spectra of the composite electrolyte before and after electrochemical cycling (Figure 7d), significantly increased intensity for the LLZO peak and a slight increase for the interfacial peak in the ^{6}Li spectrum of the cycled composite electrolyte can be clearly identified. The peak intensity can be further quantified based on spectral simulation, where 39% and 6% increments were calculated for the peak intensity of LLZO and the garnet–PEO interface, respectively, while no increase in intensity was allotted to the PEO phase. The results indicate that the Li^{+}-diffusion pathway is mainly through the LLZO particles. Given these insights, NMR is a powerful tool to study Li-ion transport in various local structural environments, especially composite electrolytes. In contrast, for a single-phase SSE or interface study, the information from NMR spectrum is more limited.

4.3. Neutron Depth Profiling

The high sensitivity to elements with a low atomic number such as Li, B, Na, etc.,[57–59] makes neutron-based techniques powerful tools for studying batteries. Neutron depth profiling (NDP) based on the stoichiometric nuclear reaction between neutrons and the isotope ^{6}Li: $^{6}Li + n \rightarrow {}^{4}He$ (2055 keV) + ^{3}H (2727 keV)[57,58] is a particularly sensitive and selective technique to analyze Li distributions and transport. In essence, this technique enables quantitative measurement of Li abundance with detailed depth profiles. Because of the unique opportunities this method facilitates, NDP has been used to measure Li transport in Li-ion batteries in situ.[60–62] Recently, Hu and co-workers used in situ NDP to monitor Li plating–stripping behavior near the garnet–electrode interfaces in real time (**Figure 8**a,b).[63] Because of the poor contact with the garnet SSE, the Li/garnet/CNT asymmetric cell showed less reversibility in Li plating–stripping than the Li/garnet/Li symmetric cell. The depth dependence of the distribution of Li also enabled more detailed analysis of the Li^{+}-transport behavior through electrode materials, at interfaces, and in near-surface garnet SSE, which can provide feedback for future interface engineering approaches and improve the performance of garnet-based solid-state batteries.

The most useful and powerful aspect of in situ NDP is its ability to diagnose short-circuits in Li/garnet/Li symmetric cells. The symmetric cell is a common strategy to study the stability and high-current-density cyclability of SSEs, since the high interfacial resistance at the cathode impedes high-rate cycling of full-cell compositions. However, for a symmetric cell, it is challenging to identify a small or subtle short-circuit after high-current-density cycling, given the nature of the voltage profile. The diagnosis can be further complicated by mixed electronically–ionically conductive states or partial short-circuits in SSEs, which limit the efficacy of conventional EIS in these cases. Recently, Albertus et al. suggested a depletion test using limited Li in test cells to identify short-circuits.[64] This method is reasonable, yet not practical, since a non-shorted cell can form a short-circuit during the depletion process due to loss of contact. The in situ NDP technique is sensitive to any non-ionic current that affects the ^{6}Li count, which makes it a

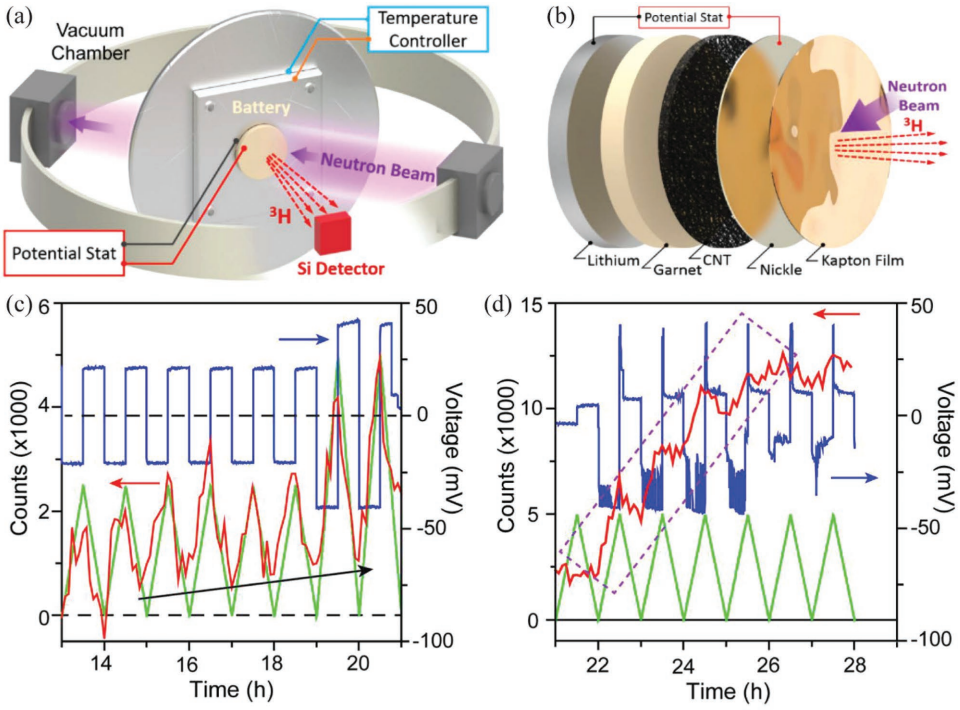

Figure 8. In situ monitoring of Li^{+} transport and battery diagnosis by NDP. a) Schematic of the NDP system. b) Cell configuration of the asymmetric cell. c,d) The zoomed-in images of the voltage profile (blue), charge curve (green), and integrated NDP count curve (red) of a symmetric cell cycling at the prediction (c) and "dynamic short-circuit" (d) stages, respectively. a–d) Reproduced with permission.[63] Copyright 2017, American Chemical Society.

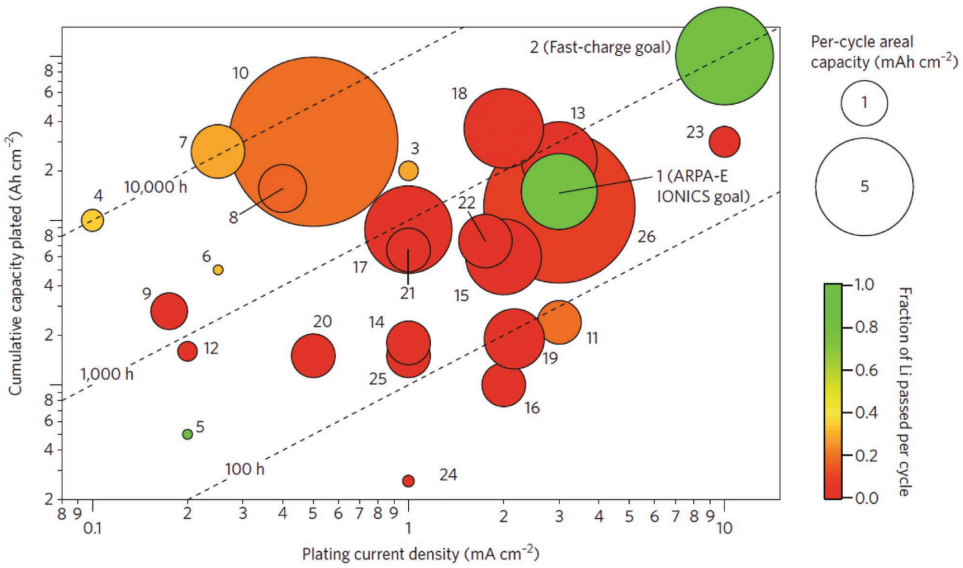

Figure 9. The status of published efforts within the field of lithium-metal batteries. Points 1 and 2 are goals, 3–6 pertain to LiPON thin-film cells, 7–9 pertain to PEO-based solid polymer electrolytes, 10–12 pertain to solid inorganic separators, 13 and 14 pertain to custom nanostructures, and 15–26 pertain to liquid electrolytes. Reproduced with permission.[64] Copyright 2018, Nature Publication Group.

powerful method to diagnose short-circuits in symmetric cells. As shown in Figure 8c,d, before the voltage profile exhibits any obvious change, the NDP curve facilitates the prediction of an imminent short-circuit. Therefore, as a quantitative technique, NDP enables an understanding of Li^+ transport and the failure modes of solid-state batteries.

5. Outlook

The application of SSEs not only addresses the safety issues associated with conventional liquid electrolytes, but also enables the utilization of better electrode materials like Li-metal anodes and high-voltage cathodes to achieve higher energy densities. Albertus et al. compared and analyzed the cumulative areal capacity, current density, per-cycle areal capacity, and the fraction of cycled Li from the total available in their work on solid-state Li-metal batteries, as shown in **Figure 9**.[64] Today's lithium-metal batteries still face many challenges including insufficient energy and power density, low utilization of available lithium while cycling, limited rate capability and stability, and unknown safety in large-format cells. Most of these challenges are fundamentally related to the solid–solid interfaces, which limits the practical application of SSEs. Current research has gradually shifted from seeking better fast ion conductors to addressing the interfacial resistance and interface stability issues of solid-state batteries. Here, we have reviewed two practical routes to improve the anode/electrolyte interface from the perspective of material selection. We have also compared several popular practices to improve the cathode/electrolyte interface. We then discussed the interfaces within the composite electrolytes and how the interfaces can be employed as fast ion pathways through rigorous structural design. Finally, we introduced several experimental characterization techniques that can effectively reveal the reactions and ion transport in solid-state batteries.

Though faced with many challenges and obstacles, Li-metal batteries still hold great potential as high-performance, reliable, and cost-efficient energy-storage solutions for the future. For the anode, ingenious modifications to the surface and active materials are needed to further reduce the interfacial resistance of the anode/electrolyte interface. In addition, studies focusing on refining the composition of and defining property–performance relationships for Li alloys could be extremely pertinent to the development of solid-state batteries. For the cathode in solid-state batteries, in addition to inserting soft and conductive interlayers in between the cathode and electrolyte, in situ synthesis and co-sintering on the garnet SSE are effective approaches that require further development. Alternatively, nanostructures for cathode–SSE architectures are also a promising route to facilitate ion transport. For the solid-state electrolyte, in addition to the persistent pursuit of higher ionic conductivity at lower operating temperatures, improving the electrochemical and mechanical performance through structural designs, especially at the nanoscale, is another interesting aspect for future research. Moreover, computational simulations are playing an increasingly important role in assisting traditional experimental characterization and have incomparable advantages in material exploration, selection, and designs. With better insights into the interfaces for solid-state batteries, a more rational approach to the design of materials and structures is anticipated.

Acknowledgements

J.D., C.Y., and C.W. contributed equally to this work.

Conflict of Interest

The authors declare no conflict of interest.

Keywords

interface engineering, lithium-metal anodes, solid-state batteries

Received: March 30, 2018
Revised: August 20, 2018
Published online: October 9, 2018

[1] A. Manthiram, X. Yu, S. Wang, *Nat. Rev. Mater.* **2017**, *2*, 16103.
[2] C. A. Geiger, E. Alekseev, B. Lazic, M. Fisch, T. Armbruster, R. Langner, M. Fechtelkord, N. Kim, T. Pettke, W. Weppner, *Inorg. Chem.* **2011**, *50*, 1089.
[3] V. Thangadurai, H. Kaack, W. J. F. Weppner, *J. Am. Ceram. Soc.* **2003**, *86*, 437.
[4] R. Murugan, S. Ramakumar, N. Janani, *Electrochem. Commun.* **2011**, *13*, 1373.
[5] J. L. Allen, J. Wolfenstine, E. Rangasamy, J. Sakamoto, *J. Power Sources* **2012**, *206*, 315.
[6] S. Ohta, T. Kobayashi, T. Asaoka, *J. Power Sources* **2011**, *196*, 3342.
[7] Y. Inaguma, C. Liquan, M. Itoh, T. Nakamura, T. Uchida, H. Ikuta, M. Wakihara, *Solid State Commun.* **1993**, *86*, 689.
[8] J.-Q. Zheng, Y.-F. Li, R. Yang, G. Li, X.-K. Ding, *Ceram. Int.* **2017**, *43*, 1716.
[9] H. Kawai, J. Kuwano, *J. Electrochem. Soc.* **1994**, *141*, L78.
[10] Z. Liu, W. Fu, E. A. Payzant, X. Yu, Z. Wu, N. J. Dudney, J. Kiggans, K. Hong, A. J. Rondinone, C. Liang, *J. Am. Chem. Soc.* **2013**, *135*, 975.
[11] E. Rangasamy, Z. Liu, M. Gobet, K. Pilar, G. Sahu, W. Zhou, H. Wu, S. Greenbaum, C. Liang, *J. Am. Chem. Soc.* **2015**, *137*, 1384.
[12] Y. Yan, R. S. Kühnel, A. Remhof, L. Duchêne, E. C. Reyes, D. Rentsch, Z. Łodziana, C. Battaglia, *Adv. Energy Mater.* **2017**, 7.
[13] R. Mohtadi, A. Remhof, P. Jena, *J. Phys.: Condens. Matter* **2016**, *28*, 353001.
[14] M. Matsuo, A. Remhof, P. Martelli, R. Caputo, M. Ernst, Y. Miura, T. Sato, H. Oguchi, H. Maekawa, H. Takamura, *J. Am. Chem. Soc.* **2009**, *131*, 16389.
[15] Y. Zhu, X. He, Y. Mo, *ACS Appl. Mater. Interfaces* **2015**, *7*, 23685.
[16] F. Han, Y. Zhu, X. He, Y. Mo, C. Wang, *Adv. Energy Mater.* **2016**, *6*, 1501590.
[17] Y. Zhao, Y. Ding, Y. Li, L. Peng, H. R. Byon, J. B. Goodenough, G. Yu, *Chem. Soc. Rev.* **2015**, *44*, 7968.
[18] N. Kamaya, K. Homma, Y. Yamakawa, M. Hirayama, R. Kanno, M. Yonemura, T. Kamiyama, Y. Kato, S. Hama, K. Kawamoto, *Nat. Mater.* **2011**, *10*, 682.
[19] L. Cheng, W. Chen, M. Kunz, K. Persson, N. Tamura, G. Chen, M. Doeff, *ACS Appl. Mater. Interfaces* **2015**, *7*, 2073.
[20] R. Sudo, Y. Nakata, K. Ishiguro, M. Matsui, A. Hirano, Y. Takeda, O. Yamamoto, N. Imanishi, *Solid State Ionics* **2014**, *262*, 151.
[21] J. van den Broek, S. Afyon, J. L. Rupp, *Adv. Energy Mater.* **2016**, *6*, 1600736.
[22] X. Han, Y. Gong, K. K. Fu, X. He, G. T. Hitz, J. Dai, A. Pearse, B. Liu, H. Wang, G. Rubloff, *Nat. Mater.* **2017**, *16*, 572.
[23] C. Wang, Y. Gong, B. Liu, K. Fu, Y. Yao, E. Hitz, Y. Li, J. Dai, S. Xu, W. Luo, *Nano Lett.* **2017**, *17*, 565.
[24] D. Lin, Y. Liu, Z. Liang, H.-W. Lee, J. Sun, H. Wang, K. Yan, J. Xie, Y. Cui, *Nat. Nanotechnol.* **2016**, *11*, 626.
[25] Y. Zhang, W. Luo, C. Wang, Y. Li, C. Chen, J. Song, J. Dai, E. M. Hitz, S. Xu, C. Yang, *Proc. Natl. Acad. Sci. USA* **2017**, *114*, 3584.
[26] Z. Liang, D. Lin, J. Zhao, Z. Lu, Y. Liu, C. Liu, Y. Lu, H. Wang, K. Yan, X. Tao, *Proc. Natl. Acad. Sci. USA* **2016**, *113*, 2862.
[27] W. Luo, Y. Gong, Y. Zhu, K. Fu, J. Dai, S. D. Lacey, C. Wang, B. Liu, X. Han, Y. Mo, E. D. Wachsman, L. Hu, *J. Am. Chem. Soc.* **2016**, *138*, 12258.
[28] C. Wang, H. Xie, L. Zhang, Y. Gong, G. Pastel, J. Dai, B. Liu, E. D. Wachsman, L. Hu, *Adv. Energy Mater.* **2018**, *8*, 1701963.
[29] K. K. Fu, Y. Gong, B. Liu, Y. Zhu, S. Xu, Y. Yao, W. Luo, C. Wang, S. D. Lacey, J. Dai, *Sci. Adv.* **2017**, *3*, e1601659.
[30] C.-L. Tsai, V. Roddatis, C. V. Chandran, Q. Ma, S. Uhlenbruck, M. Bram, P. Heitjans, O. Guillon, *ACS Appl. Mater. Interfaces* **2016**, *8*, 10617.
[31] W. Luo, Y. Gong, Y. Zhu, Y. Li, Y. Yao, Y. Zhang, K. Fu, G. Pastel, C. F. Lin, Y. Mo, *Adv. Mater.* **2017**, *29*, 1606042.
[32] B. Drevet, N. Eustathopoulos, *J. Mater. Sci.* **2012**, *47*, 8247.
[33] R. Klein, M. Desmaison-Brut, P. Ginet, A. Bellosi, J. Desmaison, *J. Eur. Ceram. Soc.* **2005**, *25*, 1757.
[34] P. Xiao, B. Derby, *Acta Mater.* **1996**, *44*, 307.
[35] M. Trybula, T. Gancarz, W. Gasior, A. Pasturel, *Metall. Mater. Trans. A* **2014**, *45*, 5517.
[36] W. Zhou, S. Wang, Y. Li, S. Xin, A. Manthiram, J. B. Goodenough, *J. Am. Chem. Soc.* **2016**, *138*, 9385.
[37] H. Duan, Y.-X. Yin, Y. Shi, P.-F. Wang, X.-D. Zhang, C.-P. Yang, J.-L. Shi, R. Wen, Y.-G. Guo, L.-J. Wan, *J. Am. Chem. Soc.* **2018**, *140*, 82.
[38] Y. Li, B. Xu, H. Xu, H. Duan, X. Lü, S. Xin, W. Zhou, L. Xue, G. Fu, A. Manthiram, J. B. Goodenough, *Angew. Chem., Int. Ed.* **2017**, *56*, 753.
[39] P. R. Chinnam, S. L. Wunder, *ACS Energy Lett.* **2017**, *2*, 134.
[40] S. Ohta, S. Komagata, J. Seki, T. Saeki, S. Morishita, T. Asaoka, *J. Power Sources* **2013**, *238*, 53.
[41] K. Park, B.-C. Yu, J.-W. Jung, Y. Li, W. Zhou, H. Gao, S. Son, J. B. Goodenough, *Chem. Mater.* **2016**, *28*, 8051.
[42] B. Liu, K. Fu, Y. Gong, C. Yang, Y. Yao, Y. Wang, C. Wang, Y. Kuang, G. Pastel, H. Xie, E. D. Wachsman, L. Hu, *Nano Lett.* **2017**, *17*, 4917.
[43] C. Wang, L. Zhang, H. Xie, G. Pastel, J. Dai, Y. Gong, B. Liu, E. D. Wachsman, L. Hu, *Nano Energy* **2018**, *50*, 393.
[44] J. Zhang, N. Zhao, M. Zhang, Y. Li, P. K. Chu, X. Guo, Z. Di, X. Wang, H. Li, *Nano Energy* **2016**, *28*, 447.
[45] L. Chen, Y. Li, S.-P. Li, L.-Z. Fan, C.-W. Nan, J. B. Goodenough, *Nano Energy* **2018**, *46*, 176.
[46] K. K. Fu, Y. Gong, J. Dai, A. Gong, X. Han, Y. Yao, C. Wang, Y. Wang, Y. Chen, C. Yan, Y. Li, E. D. Wachsman, L. Hu, *Proc. Natl. Acad. Sci.* **2016**, *113*, 7094.
[47] H. Xie, C. Yang, K. Fu, Y. Yao, F. Jiang, E. Hitz, B. Liu, S. Wang, L. Hu, *Adv. Energy Mater.* **2018**, *8*, 1703474.
[48] J. Bae, Y. Li, F. Zhao, X. Zhou, Y. Ding, G. Yu, *Energy Storage Mater.* **2018**, *15*, 46.
[49] J. Zheng, M. Tang, Y.-Y. Hu, *Angew. Chem., Int. Ed.* **2016**, *55*, 12538.
[50] W. Liu, S. W. Lee, D. Lin, F. Shi, S. Wang, A. D. Sendek, Y. Cui, *Nat. Energy* **2017**, *2*, 17035.
[51] H. Zhai, P. Xu, M. Ning, Q. Cheng, J. Mandal, Y. Yang, *Nano Lett.* **2017**, *17*, 3182.
[52] K. Fu, Y. Gong, G. T. Hitz, D. W. McOwen, Y. Li, S. Xu, Y. Wen, L. Zhang, C. Wang, G. Pastel, J. Dai, B. Liu, H. Xie, Y. Yao, E. D. Wachsman, L. Hu, *Energy Environ. Sci.* **2017**, *10*, 1568.
[53] C. Yang, L. Zhang, B. Liu, S. Xu, T. Hamann, D. McOwen, J. Dai, W. Luo, Y. Gong, E. D. Wachsman, L. Hu, *Proc. Natl. Acad. Sci. USA* **2018**, *115*, 3770.
[54] W. Zhang, D. A. Weber, H. Weigand, T. Arlt, I. Manke, D. Schröder, R. Koerver, T. Leichtweiss, P. Hartmann, W. G. Zeier, J. Janek, *ACS Appl. Mater. Interfaces* **2017**, *9*, 17835.
[55] F. Nobili, R. Tossici, R. Marassi, F. Croce, B. Scrosati, *J. Phys. Chem. B* **2002**, *106*, 3909.
[56] J. Zheng, M. Tang, Y. Y. Hu, *Angew. Chem.* **2016**, *128*, 12726.
[57] R. Downing, G. Lamaze, J. Langland, S. Hwang, *J. Res. Natl. Inst. St and. Technol.* **1993**, *98*, 109.
[58] H. Wang, R. G. Downing, J. A. Dura, D. S. Hussey, in *Polymers for Energy Storage and Delivery: Polyelectrolytes for Batteries and*

Fuel Cells (Eds: K. A. Page, C. L. Soles, J. Runt), ACS Publications, Washington, D.C., USA **2012**, p. 91.
[59] H. Liu, Y. Chen, S. Hy, K. An, S. Venkatachalam, D. Qian, M. Zhang, Y. S. Meng, *Adv. Energy Mater.* **2016**, *6*, 1502143.
[60] D. X. Liu, A. C. Co, *J. Am. Chem. Soc.* **2016**, *138*, 231.
[61] J. Oudenhoven, F. Labohm, M. Mulder, R. Niessen, F. Mulder, P. Notten, *Adv. Mater.* **2011**, *23*, 4103.
[62] S. Whitney, S. Biegalski, Y. Huang, J. Goodenough, *J. Electrochem. Soc.* **2009**, *156*, A886.
[63] C. Wang, Y. Gong, J. Dai, L. Zhang, H. Xie, G. Pastel, B. Liu, E. Wachsman, H. Wang, L. Hu, *J. Am. Chem. Soc.* **2017**, *139*, 14257.
[64] P. Albertus, S. Babinec, S. Litzelman, A. Newman, *Nat. Energy* **2018**, *3*, 16.